Scanning tunneling microscopy and spectroscopy of graphene layers on graphite

Adina Luican, Guohong Li and Eva Y. Andrei

Department of Physics and Astronomy, Rutgers University, Piscataway, New Jersey 08854, USA

Abstract:
We report low temperature scanning tunneling microscopy and spectroscopy on graphene flakes supported on a graphite substrate. The experiments demonstrate that graphite is exceptionally well suited as a substrate for graphene because it offers support without disturbing the intrinsic properties of the charge carriers. The degree of coupling of a graphene flake to the substrate was recognized and characterized from the appearance of an anomalous Landau level sequence in the presence of a perpendicular magnetic field. By following the evolution of the Landau level spectra along the surface, we identified graphene flakes that are decoupled or very weakly coupled to the substrate. From the Landau level sequence in this flake, we extract the local Fermi velocity and energy of the Dirac point and find extremely weak spatial variation of these quantities confirming the high quality and non invasive nature of the graphite substrate.

Introduction

Graphene, a one-atom thick layer of crystalline carbon possesses extraordinary electronic properties, which make it a prime candidate for novel nano-electronic devices, at the same time raising the prospect to observe phenomena hitherto unseen in bench top experiments [1-6]. These unusual properties are a consequence of the 2D honeycomb structure of graphene which imposes low energy dynamics described by the Dirac Hamiltonian and consequently the quasiparticle charge carriers mimic relativistic massless particles. The relativistic nature of the quasiparticles together with the fact that the density of states is linear and vanishes at the Dirac point, $\rho(E) \sim |E| / v_F^2$, give rise to intriguing transport and thermodynamic properties. Examples include bipolar field effect [1], perfect transmission through electrostatic barriers[2], specular Andreev reflection at a graphene superconductor interface [3], and spin carrying edge states[7].

Underlying these predictions is the assumption that the quasiparticles and the Dirac point are well defined, which would be the case if the graphene layer is minimally affected by interactions with the environment. This assumption is well justified in the case of 2D electrons inside semiconductor heterostructures where the carriers are buried deep under the surface and protected from the environment. However, in graphene the charge carriers are exposed and highly sensitive to environmental disturbances. They can interact with charged impurities and short range scatterers associated with the substrate material, with carriers introduced by adsorbed molecules and by electrical contacts. Near the Dirac point, where screening is essentially absent, these effects are particularly important as they can obscure the intrinsic properties of the relativistic charge carriers.

To date the most common substrate materials in use to support graphene correspond to two methods of sample production. One is mechanical exfoliation from bulk graphite crystals [4] followed by

deposition on SiO_2 substrates. The other is graphitization of a surface such as SiC under vacuum conditions in which case the substrate is SiC [8]. In both methods, experiments are usually carried out with one side of the graphene sample exposed and the other in direct contact with a substrate. While adsorbed molecules on the exposed surface do not measurably reduce the intrinsic mobility of the charge carriers [9], this is not the case for the side facing the insulating substrates. The insulating substrate introduces random potential fluctuations that remain unscreened upon approaching the Dirac point where the compressibility vanishes, causing the system to break up into islands of electrons and holes that follow the landscape of the random potential [10]. As a result, the Dirac point is smeared over several tens of meV (or effective gate voltage fluctuations of ~ 2V) which essentially makes it invisible in most applications involving macroscopic probes such a transport, optics or ARPES. Moreover, even in a local measurement such as STS of graphene on insulating substrates one does not observe the expected linear energy dependence of the density of states and its vanishing at the Dirac point [1]. In order to understand the physics and to exploit graphene's potential in device application one first needs to determine if and to what extent the charge carriers resemble massless Dirac fermions. To that end it is important to devise ways to isolate the graphene layers from random potential introduced by defects and trapped charges associated the insulating substrate. One way to achieve this end is to replace the insulating substrate with one that is conducting, pristine and lattice matched to graphene. Such a substrate does exist: it is graphene's parent, graphite, and as we show below it does indeed provide a supporting structure that is less invasive than SiO_2 and SiC .

Experimental method

Experiments were carried out with a home-built low-temperature (2/4 ^{0}K) high-magnetic field (13/15T) scanning tunneling microscope (STM). The STM is equipped with both coarse and fine motors allowing large area scans (mm) as well as zooming into subatomic length scales. The controller was a commercial SPM 100 unit from RHK Technologies. The sample was highly oriented pyrolitic-graphite (HOPG) cleaved in air and the STM tips were mechanically cut Pt-Ir wire. The magnetic field was applied perpendicular to the sample surface with the superconducting magnet in persistent mode. Differential conductance measurements were carried out with a lock-in technique using 450Hz a.c. modulation of the bias voltage.

Graphene on Graphite

Graphene on graphite samples were prepared by mechanical exfoliation of HOPG, but instead of the usual practice of depositing the isolated flakes on an SiO_2 substrate we focused on loose flakes left behind on the graphite surface. We could readily find graphene flakes on the surface of graphite by using the coarse scanning capability of the STM. By combining scanning tunneling microscopy and spectroscopy together with Landau level spectroscopy, we were able to identify flakes of various thicknesses and degree of coupling to the substrate. STM topography of such a flake, shown in Fig. 1a, reveals three layers separated in height by atomic steps Fig. 1b.

Decoupled graphene.

Atomic resolution topography was the first step to identify decoupled graphene flakes on the surface of graphite. The decoupled flakes exhibit the distinctive honeycomb structure of graphene (Fig. 1c), in clear

contrast to the triangular structure seen on graphite (Fig. 1d). This difference reflects the fact that STM image is sensitive to the local density of states (DOS). Therefore, although graphite consists of graphene layers each with honeycomb structure, the density of states on Bernal stacked graphite causes one (triangular) sub-lattice only to be visible in low bias STM images [11]. Once a flake with honeycomb structure is identified, we test it further with STS measurements to obtain the bias dependence of the differential conductance, a quantity directly related to the DOS [12]. For decoupled graphene flakes, we observe the distinctive signature of massless Dirac fermion quasiparticles: a V shaped DOS that vanishes at the Dirac point. We note that the Fermi energy is ~ 16.9 meV below the Dirac point, indicating a slightly hole doped sample corresponding to a carrier density of $\sim 3\times 10^{10} cm^{-2}$. For comparison we also show in Fig. 1a the spectrum of graphite, where the contribution of the Dirac cones to the DOS is overshadowed by low energy states corresponding to motion perpendicular to the layers. This gives rise to a finite density of states at the Dirac point. In contrast, for graphene deposited on insulating substrates one does not observe the intrinsic spectrum of massless Dirac fermions [13,14].

An even more stringent test of decoupled graphene becomes accessible by applying a magnetic field, B, normal to the layer and probing for the appearance of Landau energy levels. This sequence is shown in Fig. 2b for a decoupled graphene layer at 4T. To compare to the expected Landau level sequence of massless Dirac fermions[1]:

$$E_n = E_D + v_F sign(n)\sqrt{2e\hbar|n|B} \quad n = 0, \pm 1, \pm 2.. \qquad (1)$$

we plot the Landau level peak energy against the reduced variable $(|n|B)^{1/2}$ for fields up to 10T as indicated in Fig. 2c. Here E_D is the Dirac point energy measured with respect to the Fermi energy, n the level index with $n > 0$ corresponding to electrons and $n < 0$ to holes. This plot collapses all the data onto a straight line revealing a single sequence of Landau levels characteristic of massless Dirac fermions. Comparing to Eq.(1) we obtain (from the slope) the value of the Fermi velocity, $v_F = 0.79 \times 10^6$ m/s. The ~20% reduction compared to the accepted Fermi velocity can be attributed to electron-phonon interactions as discussed in reference [15]. In addition, we find the position of the Dirac energy relative to the Fermi level, $E_D = 16.6$ meV, is consistent with that in the zero-field data (Fig.2a).

The field-independent Landau level at zero energy is a consequence of the chirality of the Dirac fermions and does not exist in other known 2d electron system such as electrons on helium or in GaAs heterostructures where the excitations are non-relativistic massive quasiparticles. Indirect evidence of this level in graphene on SiO_2 substrates was gleaned from Quantum Hall Effect measurements where the usual Quantum Hall plateaux at zero filling factor is replaced by a step [5,6]. A comparison between the spectra of decoupled graphene and graphite in a field of 4T (Fig. 2b) shows that the sharp Landau level sequence seen in graphene is absent on the graphite surface. These results demonstrate that the charge carriers in graphene are indeed Dirac fermions and that their properties become apparent and accessible to the STM probe on a minimally intrusive substrate like graphite.

Coupled graphene layers.

Once a graphene sheet couples to the underlying graphite layers its properties change dramatically [16]. To study the effect of variations in coupling strength we followed the spatial evolution of the Landau level sequence across the flake shown in Fig. 3a. This flake consists of two regions separated by a diagonal ridge. Above the ridge in region A, the flake consists of a single graphene layer decoupled from

the substrate as determined by the criteria discussed above. The spectral features in region B below the ridge show neither characteristics of single layer graphene nor those of graphite, but as we show below, they are consistent with a very weakly coupled layer. To study the spatial evolution, we recorded Landau level spectra at a field of 4T on a 32x32 point grid covering the entire area shown in Fig. 3a. Typical spectra from both region A and B are presented In Fig. 3b. We note that in region A the Landau Level sequence is characteristic of decoupled graphene as seen from the scaling of the peak energy with $|n|^{1/2}$ in Fig. 3c . In region A the spectra are the same at all points, but once the ridge is crossed into region B the spectra undergo a qualitative change.

In Fig. 4 we compare the Landau level spectra in regions A and B and illustrate their spatial evolution. We chose a coordinate system (Fig. 4a) with the abscissa coinciding with the ridge and the ordinate representing the distance from it. In this representation all the points in region A are above the x axis and points in region B are below it. In Fig. 4b we show averaged Landau level spectra taken along lines with constant distance from the ridge. In this figure, the y-axis represents the distance from the ridge and the x-axis is the energy.

We find that the Landau levels in region A correspond to decoupled single layer graphene as discussed above. In contrast the Landau levels in region B are slightly shifted towards the Dirac point and their level index dependence is not the one expected for neither bilayer or multilayer graphene [1, 17, 19]. To understand the level sequence in region B we compare to calculations by Pereira et al. [18], showing the evolution of the Landau level sequence of a bilayer as a function of interlayer coupling strength. They find that as the coupling strength is increased the spectrum evolves from that of a single uncoupled graphene layer into a sequence where each Landau level (except n=0) splits as the twofold degeneracy is lifted with increasing coupling strength. For any given coupling strength this gives rise to a unique Landau level sequence. We used this model to interpret the Landau level sequence in region B. In Figs. 4c and 4d we compare the experimental data to predictions from this model. Here the vertical axis is energy and the horizontal axis on the right is the interlayer coupling, t. In [18], the evolution of Landau level energies with interlayer coupling depends on the Fermi velocity and on the magnetic field. In this data the magnetic field was 4T and the Fermi velocity and coupling constant were adjusted to obtain the best fit between the measured Landau level sequence and the model.

In Fig. 4c, we show that the Landau level sequence in region A matches that of a decoupled layer (or zero coupling in the model) and Fermi velocity of $v_F^e = (0.80\pm0.05) \times 10^6$ m/s and $v_F^h = (0.78\pm0.05) \times 10^6$ m/s for electrons and holes respectively.

In Fig. 4d the sequence in region B is shown to match the theoretical model for interlayer coupling t= (40±5) meV, one order of magnitude smaller than the coupling constant in graphite. The Fermi velocity is $v_F^e = (0.80\pm0.05) \times 10^6$ m/s and $v_F^h = (0.80\pm0.05) \times 10^6$ m/s on the electron and hole branches, respectively. We conclude that the anomalous Landau level sequence in region B reflects a small but finite interlayer coupling.

Turning our attention to the single layer Landau level sequence in region A, we can use the sequence to extract the local Fermi velocity and the Dirac energy as shown in Fig. 3c. Since the data were taken on a grid of points across the sample, the spatial variation of these quantities can be calculated. Fig. 5 shows the maps obtained with a spatial resolution of 9nm. The top images represent maps of the Fermi velocity calculated from fitting the Landau level sequence to equation 1 for holes (left) and electrons (right). The average values and standard deviation, $v_F^e = (0.78\pm0.05) \times 10^6$ m/s and $v_F^h = (0.75\pm0.05) \times 10^6$

m/s for electrons and holes respectively indicate that the Fermi velocity does not vary significantly across the area investigated. In Fig. 5b we show maps of the Dirac point energy obtained from the same fit. The average Dirac energy is E_D^e= (22±5) meV and E_D^h= (16±5) meV for electrons and holes respectively. The variation of the Dirac point across the sample is comparable to that in suspended graphene [19] but much smaller than on SiO_2 or SiC where the variation in the best samples exceeds ~ 40meV.

In summary, the scanning tunneling experiments described here demonstrate that graphite is exceptionally well suited as a substrate for supporting graphene. Because graphite offers support without interference, it allows accessing and studying the intrinsic properties of the charge carriers in graphene. The experiments show that the degree of coupling of graphene to the graphite substrate can be recognized and characterized from the appearance of an anomalous Landau level sequence. Here we compared Landau level spectra in two regions of graphene and showed that one was decoupled from the substrate while the other was weakly coupled to it. In both regions, we found very weak spatial variation of the Fermi velocity and of the Dirac point confirming the high quality and non-invasive nature of this substrate.

References

1. A.H. Castro Neto, F. Guinea, N.M.R. Peres, K.S. Novoselov, A.K. Geim, Rev. Mod. Phys. 81 (2009) 109.
2. M. I. Katsnelson, K. S. Novoselov, A. K. Geim, Nat. Phys. 2 (2006) 620.
3. W. J. Beenakker, Rev. Mod.Phys. 80 (2008) 1337.
4. K. S. Novoselov, A. K. Geim, S. V. Morozov, D. Jiang, Y. Zhang, S. V. Dubonos, I. V. Grigorieva, A. A. Firsov, Science 306 (2004) 666.
5. K. S. Novoselov, A. K. Geim, S. V. Morozov, D. Jiang, M. I. Katsnelson, I. V. Grigorieva, S. V. Dubonos, A. A. Firsov, Nature 438 (2005) 197.
6. Y. B. Zhang, Y. W. Tan, H. L. Stormer, P. Kim, Nature 438 (2005) 201.
7. D. A. Abanin, P. A. Lee, L. S. Levitov, Phys. Rev. Lett. 96 (2006) 176803.
8. C.Berger, Z.M. Song, T.B.Li, X.B.Li, A.Y.Ogbazghi, R.Feng, Z.T.Dai, A.N.Marchenkov, E.H.Conrad, P.N.First and W.A.de Heer, J. Phys. Chem. B 108(2004) 19912.
9. F. Schedin, K.S. Novoselov, S.V. Morozov, D. Jiang, E.H. Hill, P. Blake, A.K. Geim, Detection of Individual Gas Molecules by Graphene Sensors. cond-mat/0610809.
10. J. Martin, N. Akerman, G. Ulbricht, T. Lohmann, J. H. Smet, K. v. Klitzing, A. Yacoby, Nat. Phys. 4 (2008) 144.
11. S. Gwo, and C.K .Shih, Phys. Rev. B 47 (1993) 13059.
12. J. Tersoff and D.R Hamann, Phys. Rev. B 31 (1985) 805.
13. G. M. Rutter, J. N. Crain, N. P. Guisinger, T. Li, P. N. First, J. A. Stroscio, Science 317 (2007) 219.
14. Y. Zhang, V. W. Brar, F. Wang, C. Girit, Y. Yayon, M. Panlasigui, A. Zettl, M. F. Crommie, Nat. Phys. 4

(2008) 627.

15. G. Li, A. Luican, E. Y. Andrei, arXiv:0803.4016. (2008).
16. F. Guinea, A.H. Catro Neto, N.M. Peres, Solid State Commun. 143(2007) 116.
17. G. Li , E.Y. Andrei, Nat. Phys. 3 (2007) 623.
18. M. Pereira, F.M.Peeters, P. Vasilopoulos, Phys. Rev. B 76 (2007) 115419.
19. X. Du, I. Skachko, A. Barker, E.Y. Andrei, Nat. Nano. 3 (2008) 491.
20. E. McCann, V. I. Fal'ko, Phys. Rev. Lett. 96 (2006) 086805.

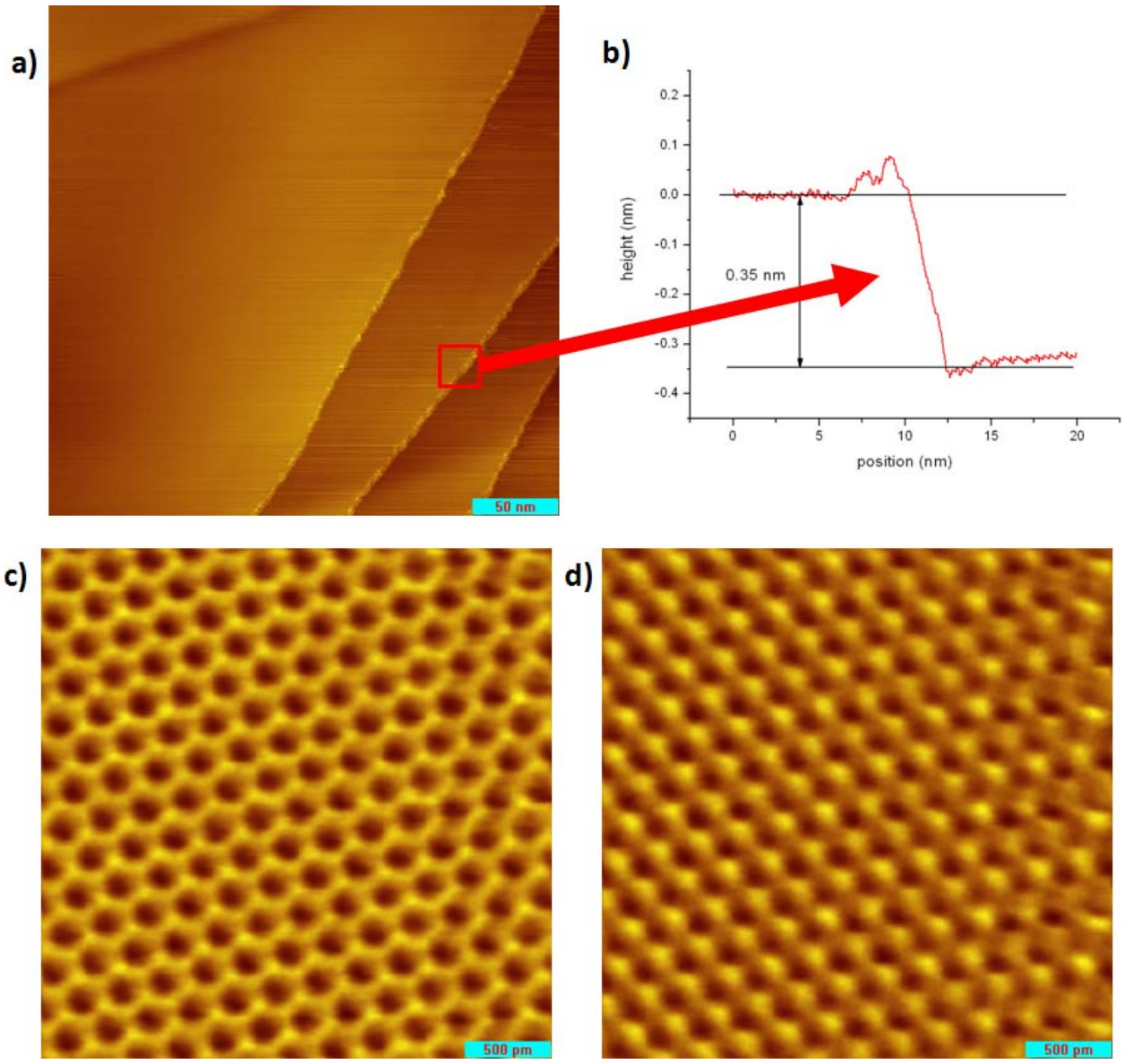

Fig. 1. Graphene flake on graphite. (a) topography of three-layer flake. (b) height profile showing separation of atomic layers. (bottom) Atomic resolution topography of (c) decoupled graphene layer showing honeycomb structure and (d) graphite.

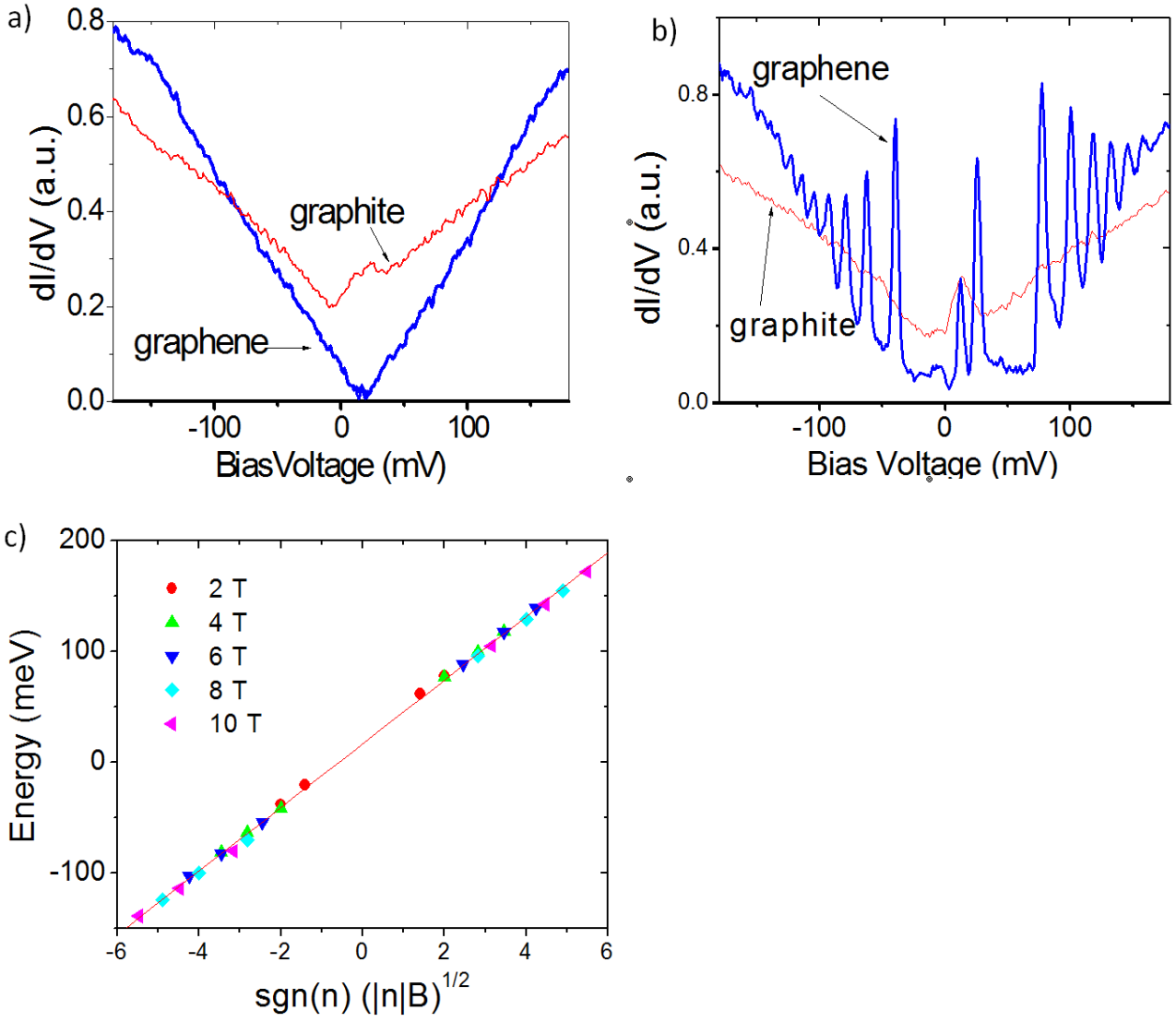

Fig. 2. (a) Spectrum of a graphene flake (blue) compared to graphite (red). (b) STS of graphene and graphite at 4T showing pronounced Landau level structure in graphene and its absence on graphite. (c) Landau level peak positions plotted against the reduced parameter $\left(|n|B\right)^{1/2}$ showing the expected scaling for massless Dirac fermions described by Eq. (1).

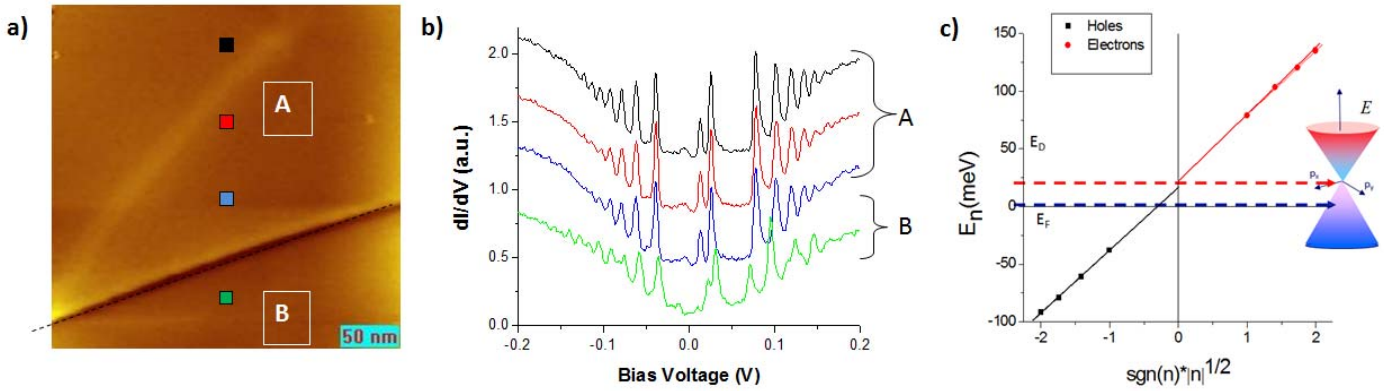

Fig. 3. (a) Topography of the investigated area showing two graphene regions, A and B, with different coupling strength to the substrate. (b) STS data showing Landau Level sequences at various positions in region A and B. (c) Linear dependence of Landau level energies, E_n , in region A on $\mathrm{sgn}(n)\sqrt{|n|}$, with n the level index.

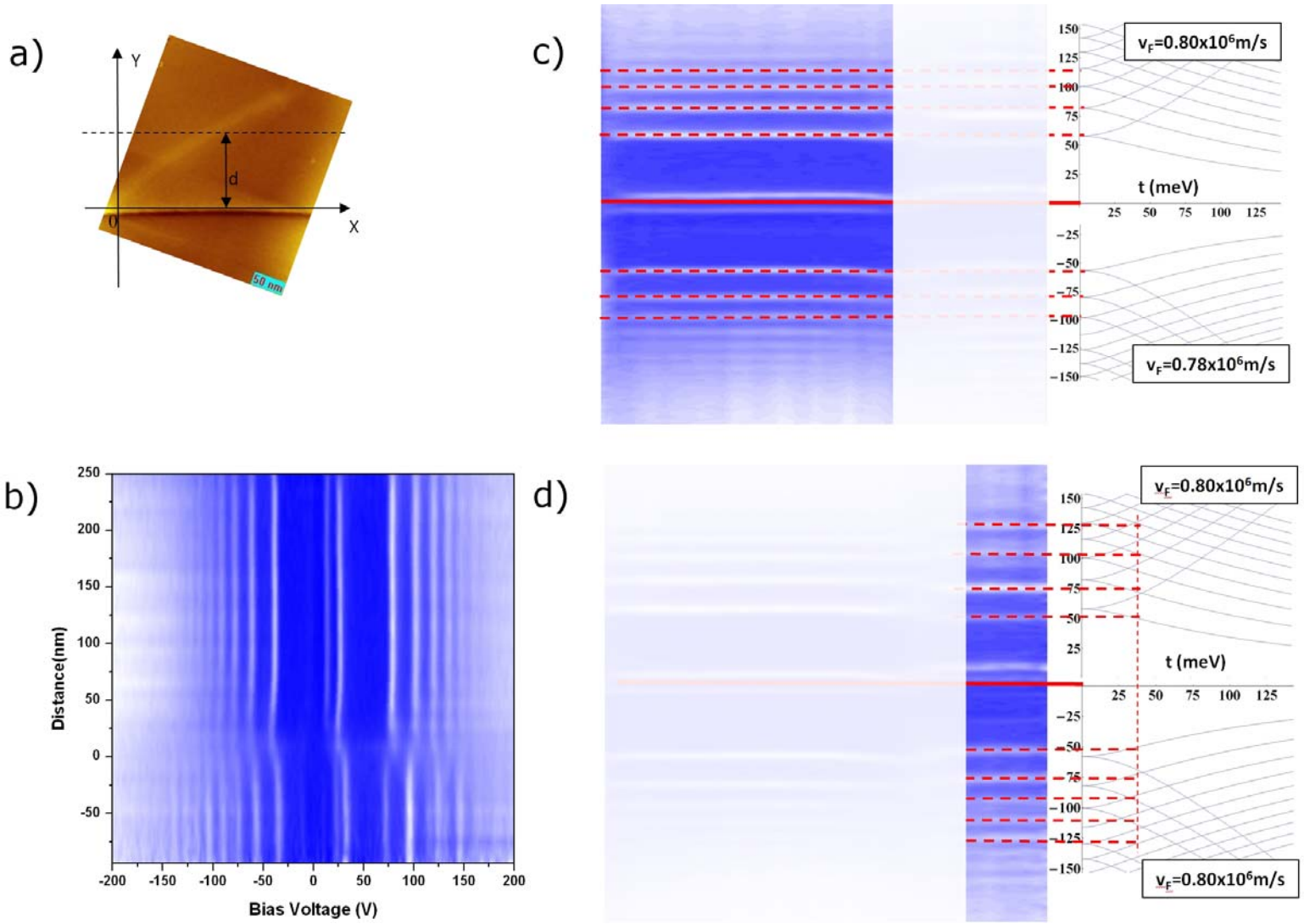

Fig. 4. (a) Topographic image of sample showing coordinate system with abscissa along the ridge separating regions A and B. (b) Intensity map of Landau level sequence showing their evolution with distance from the border between regions A and B. (c) and (d) Comparison of the experimental Landau Levels (left map) to theoretical predictions for LL evolution with interlayer coupling [18] in region A (Fig.4c) and B (Fig.4d). For clarity, in both images, the area, which is not used for the fit, is hidden.

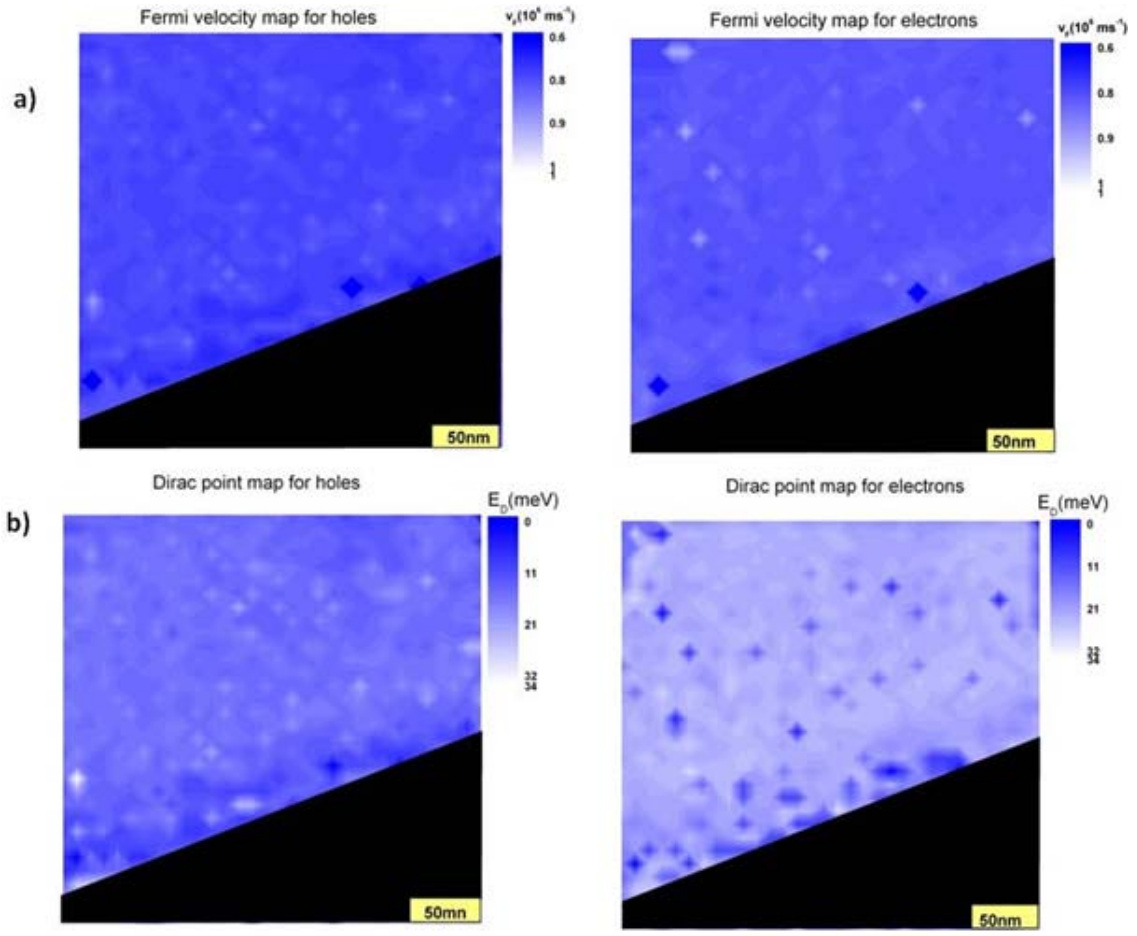

Fig. 5. (a) Map showing spatial variation of the Fermi velocity for single layer graphene in region A. (b) Map showing spatial variation of the Dirac point for the single layer graphene in region A.